Jia *et al. Horticulture Advances* (2026) 4:20
https://doi.org/10.1007/s44281-026-00107-9

Horticulture Advances

RESEARCH ARTICLE Open Access

Integrative metabolome and transcriptome analyses reveal metabolomic variations underlying fruit quality during ripening of kiwifruit (*Actinidia arguta*)

Yun Jia[1], Fangbing Ding[1], Xu Qiang[2], Meng Wang[2], Ting Ren[1], Fengwei Wang[1], Yongpeng Wu[1], Lei Zhang[1], Yu Zhao[1], Yaling Wang[1], Yanchang Wang[3] and Ying Zhang[1*]

Abstract

Kiwifruit (*Actinidia arguta*) is an economically important horticultural crop worldwide with remarkably high nutritional value. However, the dynamic metabolic changes underlying fruit quality during kiwifruit ripening remain poorly understood. In this study, integrated metabolomic and transcriptomic analyses were conducted to explore the molecular basis of fruit quality across three ripening stages in three *A. arguta* varieties with distinct flesh characteristics: 'Kokuwa' (full-green flesh), 'Xianziguang' (red flesh), and 'Qinghuang' (yellow flesh). A total of 371 differentially accumulated metabolites and their coexpressed genes were classified into six distinct metabolite *vs* gene modules. Several metabolites, including five sugars, eight organic acids, four volatile compounds, and seventeen flavonoids, such as anthocyanins, procyanidins, and flavones, were further identified as key contributors to fruit quality formation. By integrating gene coexpression network analysis with metabolomic data, we identified a range of ripening-related genes and transcription factors involved in the biosynthesis of sugars, organic acids, anthocyanins, and the L-ascorbic acid metabolic pathway. Notably, thirteen structural genes involved in anthocyanin biosynthesis—anthocyanidin reductase (2), dihydroflavonol 4-reductase (4), flavonol synthase (5), and phenylalanine ammonia-lyase (2), were strongly correlated with multiple transcription factors, indicating that a complex regulatory network governed anthocyanin biosynthesis in *A. arguta*. This study provides new insights into the molecular basis of metabolite variation in kiwifruit and highlights the potential of genetic information for improving fruit quality.

Keywords *Actinidia arguta*, Anthocyanin, Kiwifruit, Metabolic regulatory network, Multiomics, Transcription factor

Introduction

Fruit quality is a vital breeding target that strongly affects consumer appreciation and market competitiveness (Zhang et al. 2020b; Wang et al. 2021a, b). Key quality attributes are typically linked to characteristics such as color, taste (including sweetness and acidity), and nutrient content (Chen et al. 2020; Tang et al. 2020; Wu et al. 2022). However, improving fruit quality is a complex task and remains a significant challenge in both the fruit breeding and biotechnology (Shu et al. 2023). Fruit development and ripening are intricate, tightly regulated metabolic processes governed by key metabolites

*Correspondence:
Ying Zhang
zy@xab.ac.cn
[1] Xi'an Botanical Garden of Shaanxi Province (Institute of Botany of Shaanxi Province), Xi'an 710061, People's Republic of China
[2] Key Laboratory of Resource Biology and Biotechnology in Western China, Ministry of Education, College of Life Sciences, Northwest University, Xi'an 710069, People's Republic of China
[3] Wuhan Botanical Garden, Chinese Academy of Sciences, Wuhan 430074, People's Republic of China

© The Author(s) 2026. **Open Access** This article is licensed under a Creative Commons Attribution 4.0 International License, which permits use, sharing, adaptation, distribution and reproduction in any medium or format, as long as you give appropriate credit to the original author(s) and the source, provide a link to the Creative Commons licence, and indicate if changes were made. The images or other third party material in this article are included in the article's Creative Commons licence, unless indicated otherwise in a credit line to the material. If material is not included in the article's Creative Commons licence and your intended use is not permitted by statutory regulation or exceeds the permitted use, you will need to obtain permission directly from the copyright holder. To view a copy of this licence, visit http://creativecommons.org/licenses/by/4.0/.

Springer

and their underlying regulatory networks (Wang et al. 2022; Wu et al. 2022; Shu et al. 2023; Zeng et al. 2025). Consequently, a systematic exploration of the genetic foundations of metabolite biosynthesis involved in fruit formation will offer valuable insights to support fruit breeding for improved fruit quality.

Kiwifruit (*Actinidia*) is among the most economically important horticultural crops; it originated in China and is now widely cultivated in temperate regions (Huang et al. 2013). Commercial cultivars primarily originate from two species, *A. chinensis* and *A. deliciosa*, because of their diverse flesh colors (e.g., green, yellow, and red), distinctive flavors, and extended shelf life (Zhang et al. 2010; Dias et al. 2020; Popowski et al. 2021). Given the crucial role of metabolites in kiwifruit quality, recent advances in multi-omics approaches—such as high-resolution metabolomic and comprehensive transcriptomic profiling—have proven effective for identifying regulatory genes involved in flavor- and nutrition-related metabolic pathways. For instance, variations in soluble sugars, organic acids, and underlying regulatory networks throughout the kiwifruit growth cycle have been widely investigated through integrated metabolome and transcriptome analyses of *A. chinensis* cv. 'Hongyang' (Zhang et al. 2020a; Wang et al. 2022; Shu et al. 2023; Zeng et al. 2025). L-ascorbic acid (AsA) content varies among *Actinidia* species, and several structural genes and transcription factors (TFs), such as ERF, MYB, and bZIP, are involved in AsA accumulation (Chen et al. 2021; Liu et al. 2022; Shu et al. 2023). More recently, fruit coloration—an important quality trait—has been elucidated through the integration of large datasets encompassing pangenomes, metabolomes, and transcriptomes (Wang et al. 2024). Some novel structural variations (SVs) and TFs have been verified to be critical for modulating anthocyanin, chlorophyll, and carotenoid metabolism (Nardozza et al. 2020; Liu et al. 2021; Wang et al. 2024). Although key metabolites and regulatory genes affecting the quality of economically important varieties (e.g., *A. chinensis* cv 'Hongyang' and *A. chinensis* var. *deliciosa*) are well documented, the mechanisms governing metabolite accumulation in other kiwifruit species remain largely unknown.

Actinidia arguta, commonly called 'Ruanzaozi', is a geographically widespread liana with variable ploidy (4×, 6×, 8×, etc.) in natural populations that produces small, edible fruits with smooth, hairless skin (Kataoka et al. 2010; Zhang et al. 2019; Lu et al. 2022). Owing to its distinguishable appearance, flavor and the highest rates of anthocyanin, *A. arguta* has been cultivated as an important horticultural fruit in localized kiwifruit production (Li et al. 2018; Lu et al. 2022). Extensive research has been performed in recent years to assess the nutrient and flavor compositions of *A. arguta* fruits, including those of sugars and organic acids (Lin et al. 2022; Qiang et al. 2025), anthocyanins (Li et al. 2018, 2025; Tan et al. 2021; Jia et al. 2023), vitamin C (Pérez-Burillo et al. 2018) and other antioxidant metabolites (Wojdyło and Nowicka 2019; Yu et al. 2020; Hou et al. 2023). Recently, several mechanisms have been proposed to characterize key biosynthetic genes that regulate enzymes and their associated regulatory networks in *A. arguta*. Lu et al. (2024) employed integrated multiomics and population genomics analysis to identify genes related to important agronomic traits (e.g., dioecism and postharvest ripening) in *A. arguta*. Researchers have also investigated flesh color inheritance and identified several related candidate miRNAs and TFs in *A. arguta*. miR858 and AaERF059 have been reported to influence flesh color by regulating anthocyanin biosynthesis (Li et al. 2019a, b; Li et al. 2025). Additionally, AaMYBC1 interacts with AaWRKY44 to dynamically modulate anthocyanin and proanthocyanidin levels, thereby maintaining flavonoid balance (Peng et al. 2020). Although several multiomic studies of *A. arguta* have been conducted, most have focused on the effects of genetic variation on fruit quality among varieties. Consequently, the metabolic dynamics and underlying regulatory networks that govern overall fruit quality are rarely investigated throughout fruit development and ripening.

In this study, we performed a multiomics analysis and generated metabolome and transcriptome data for three *A. arguta* varieties with distinct flesh characteristics: full-green-fleshed 'Kokuwa' (KKW), red-fleshed 'Xianziguang' (XZG), and yellow-fleshed 'Qinghuang' (QH) at three fruit ripening stages. By integrating transcriptomic data with metabolite-based assessments of fruit quality, we constructed a regulatory network modulating the production and accumulation of sugars, organic acids, anthocyanins and AsA. Additionally, we identified several TFs that regulate kiwifruit quality metabolism through key metabolites and gene coexpression networks. Collectively, the findings of this study provide new insights into the mechanisms driving differences in kiwifruit metabolites and underscore the potential of genetic data for improving fruit quality.

Materials and methods

Plant materials

Three kiwifruit (*A. arguta*) varieties with distinct flesh characteristics were used in this study, namely, *A. arguta* 'KKW', 'XZG', and 'QH'. They were grown in a kiwifruit germplasm resource nursery at the Institute of Botany of Shaanxi Province (Xi'an, China). Fruits were randomly sampled based on size and skin color from three replicate lianas at three developmental stages: May 15th (early

fruit, T1), June 19th (fruit ripening, T2), and September 15th (fully ripe, T3). All the samples were rapidly frozen in liquid nitrogen and stored at −80 °C for RNA extraction and metabolite profiling.

Metabolome profiling and analysis

Metabolomic profiling was conducted by MetWare Biotechnology Co., Ltd. (Wuhan, China) utilizing a widely targeted metabolome approach, as outlined by Zhang et al. (2022). Briefly, kiwifruit pulp samples were first freeze-dried using a vacuum lyophilizer apparatus (Scientz-100F, Ningbo Scientz Biotechnology Co., Ltd., Ningbo, China) and then ground into fine powder with a mixer mill (MM 400, Retsch GmbH, Haan, Germany) containing zirconia beads at 30 Hz for 1.5 min. Approximately 100 mg of the powdered samples were extracted with 1.2 ml of 70% aqueous methanol, stirred for 30 s every 30 min (repeated six times), and centrifuged at 12,000 × g for 10 min at 4 °C overnight. The supernatants were filtered through a 0.22 μm Millipore filter and collected for analysis with a UPLC–ESI–MS/MS system (SHIMADZU Nexera X2, Shimadzu Corporation, Kyoto, Japan; MS, QTRAP 4500, AB Sciex, Framingham, MA, USA). Metabolite spectra were acquired on an AB Triple TOF 6600 mass spectrometer (AB SCIEX, Massachusetts, USA) with electrospray ionization (ESI) in both positive and negative ion modes. Metabolites were quantified on a relative basis using normalized peak areas from scheduled multiple reaction monitoring (MRM) and annotated with the self-built MetWare database. To further ensure data reliability, four quality control samples were prepared by pooling 10 mL from each experimental sample.

Principal component analysis (PCA) and hierarchical clustering were performed utilizing the prcomp function and ComplexHeatmap package (Gu et al. 2016) in R (R Core Team 2023), respectively, for both the metabolomic and transcriptomic datasets. Differentially accumulated metabolites (DAMs) among different varieties were identified by a fold change ≥ 2 or ≤ 0.5, a variable importance in the project ≥ 1 and a false discovery rate (FDR) < 0.05. To elucidate metabolic dynamics during kiwifruit ripening, the identified DAMs were subjected to clustering analysis and Kyoto Encyclopedia of Genes and Genomes (KEGG) enrichment analysis using mfuzz with the R package clusterProfiler v4.0 (Wu et al. 2021).

RNA-seq and analysis

Total RNA was extracted from the three *A. arguta* varieties at three developmental stages (three replicates per stage). In total, 27 RNA libraries were constructed and sequenced on the Illumina HiSeq platform. The clean reads were generated from the raw reads by filtering adaptor trimming, low-quality reads, and short reads utilizing FASTP v.0.22.0 (Chen et al. 2018) and subsequently aligned to the kiwifruit genome (*A. arguta* 'M1') (Lu et al. 2024) using HISAT2 v2.0.5 with default parameters (Kim et al. 2015). The raw sequencing data were deposited in the NCBI Sequence Read Archive under accession number PRJNA1222102.

Gene expression levels for each sample were quantified using HTSeq v2.0 (Putri et al. 2022), and fragments per kilobase of transcript per million mapped reads (FPKM) were calculated for each gene on the basis of transcript length. Differentially expressed genes (DEGs) with a $|\log_2(\text{fold change})| \geq 1$ and FDR < 0.05 were screened using DESeq2 v1.18.0 (Trapnell et al. 2012). Gene set enrichment analysis (GSEA) of the DEGs was further employed to evaluate enrichment of the KEGG gene sets. The GSEA was executed utilizing clusterProfiler v4.0 (Wu et al. 2021) and GseaVis v0.0.5 (ClusterGVis; https://github.com/junjunlab/ClusterGVis). Additionally, the major TF families were determined utilizing iTAK v1.7a (Zheng et al. 2016).

Integrated metabolomic and transcriptomic analyses

DEGs among the three ripening stages were used to construct gene coexpression networks through weighted gene coexpression network analysis (WGCNA) (Langfelder and Horvath 2008). The soft-thresholding value for the signed network was set to 12, ensuring a scale-free topology model with a fitting index (R^2) greater than 0.8, as determined on the basis of scale-free topology criteria. Modules were identified with a minimum module size of 30 and a moderate cluster splitting sensitivity (deepSplit = 2). The correlations between genes within each module and DAMs associated with fruit quality (sugars, organic acids, anthocyanins/proanthocyanidins, flavonoids and AsA) were subsequently analyzed to identify key regulatory modules.

Construction of the kiwifruit metabolic regulatory network

Metabolic regulatory networks were created by integrating the Pearson correlation coefficient (PCC > 0.9, $P < 0.05$) between structural genes and TFs and metabolite-associated fruit quality. Regulatory networks were constructed with CYTOSCAPE v3.7.1 (Kohl et al. 2011). In addition, we selected six genes (*L-ascorbate peroxidase 1*, *AaAPX1*; *AaAPX2*; *AaAPX3*; *AaSWEET1*; *AaSWEET2*; and *anthocyanidin reductase*, *AaANR*) on the basis of their correlation with key metabolites and validated them by quantitative reverse transcription PCR (qRT–PCR) across the three *A. arguta* varieties. A Bio-Rad CFX96 Touch Real-time PCR System (Hercules, CA, USA) was utilized for qRT–PCR analysis with SYBR Green PCR Master Mix (Takara, Kyoto, Japan) with three biological replicates. The results were

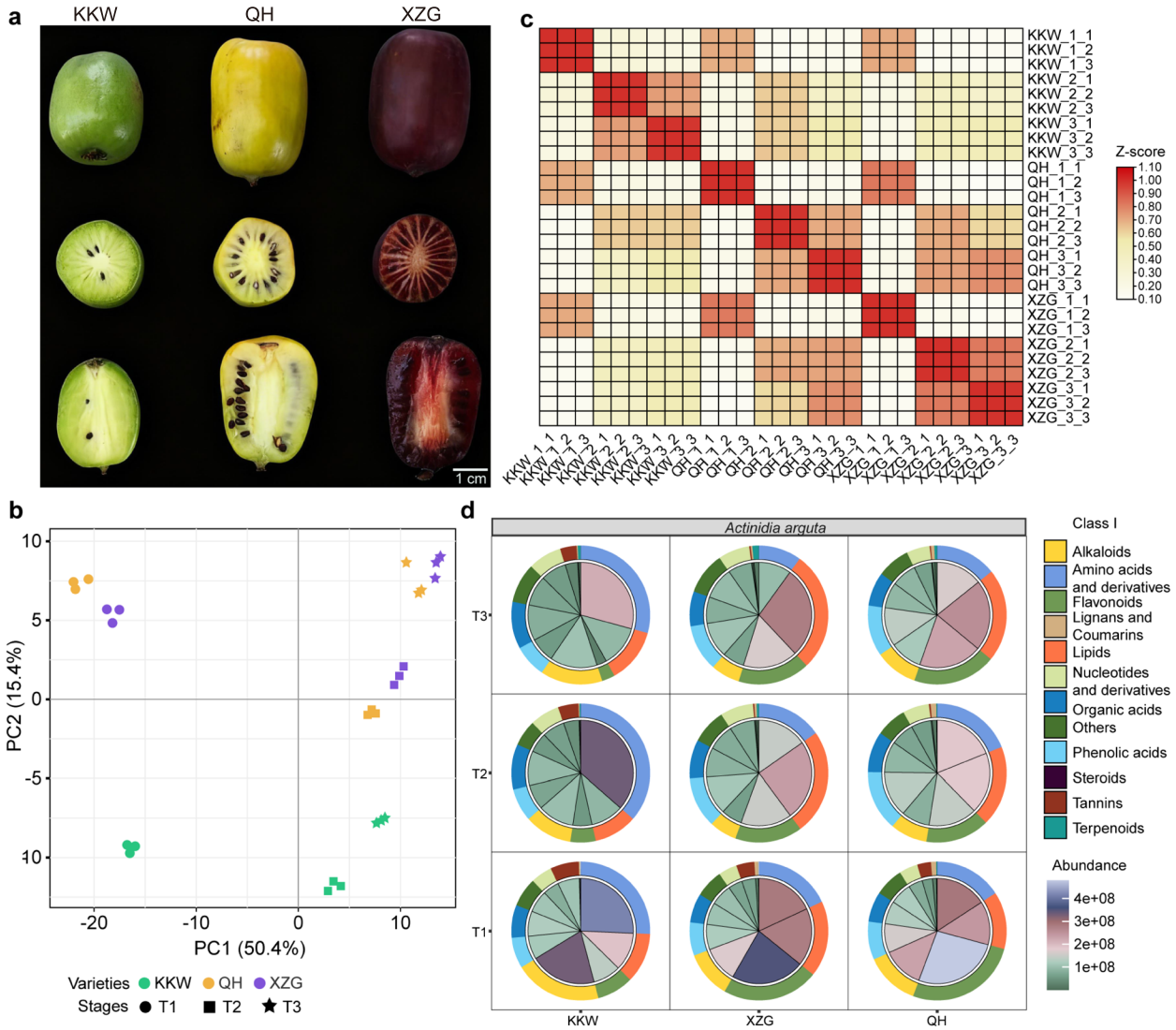


Fig. 1 Metabolic profiles of kiwifruit (*Actinidia arguta*) at three ripening stages. **a** Fruit morphology of kiwifruit varieties from 'Kokuwa' (KKW, full-green flesh), 'Qinhuang' (QH, yellow), and 'Xianziguang' (XZG, red). **b** Principal component analysis (PCA) of metabolome data. **c** Repeated correlation quality of metabolites. **d** Numbers and classification of the annotated metabolites. T1, T2, and T3 represent kiwifruit samples at the early fruit stage, fruit ripening stage, and fully ripe stage, respectively

processed using the $2^{-\Delta\Delta Ct}$ method, and the relative expression levels were normalized to those of Actinidia β-actin (Ampomah-Dwamena et al. 2009).

Statistical analysis

Significant differences were analyzed using Student's *t*-test in R ($^{*}P < 0.05$, $^{**}P < 0.01$, and $^{***}P < 0.001$). All data were obtained from three biological replicates and are presented as the mean ± standard deviation (SD).

Results

Metabolomic profiles during kiwifruit ripening

To investigate the metabolic dynamics and the relevant regulatory networks involved in the ripening process of kiwifruit, the pulp tissues of three *A. arguta* varieties (Fig. 1a) were collected at three distinct stages (T1 to T3). Throughout the growth cycle, KKW maintained green pulp, XZG pulp turned red at full ripeness (T3), and QH pulp exhibited a sequence from light-red at T1 to green at T2, and finally yellow at T3. We then monitored the changes in metabolites utilizing broadly targeted LC–MS/MS-based metabolic profiling. A total of 708 metabolites were detected and annotated in *A. arguta*,

including 132 lipids, 116 phenolic acids, 98 flavonoids, 88 amino acids and derivatives, 64 organic acids, 53 nucleotides and derivatives, 50 alkaloids, 23 lignans and coumarins, 16 tannins, 9 terpenoids, 1 steroid, and 58 other compounds (Fig. S1). PCA revealed a distinct separation among developmental stages, indicating stage-specific metabolic profiles (Fig. 1b). Hierarchical clustering also grouped samples according to ripening stage (Fig. 1c), and high correlations among the three biological replicates confirmed data reproducibility. Intriguingly, compared with those in the two tetraploid varieties XZG and QH, the accumulation patterns of metabolites in octoploid KKW significantly differed (Fig. 1d). For instance, metabolites such as alkaloids, amino acids and their derivatives, as well as tannins, were found to accumulate preferentially in KKW, while XZG and QH presented significantly higher levels of flavonoids, lipids, and phenolic acids in their pulp (Fig. 1d).

Changes in metabolites during the ripening of *A. arguta*

To further investigate metabolic dynamics during fruit ripening, 371 identified DAMs were divided into six distinct clusters (C1–C6) on the basis of their accumulation patterns (Fig. 2). We identified 114 metabolites whose contents increased (C1–C3) and 255 metabolites whose levels decreased (C4–C6) during the ripening process (Fig. 2). Metabolites abundant at the early stage (T1) were largely distinct from those detected at later stages (T2 and T3), and similar trends in relative abundance between T1 and T2/T3 were observed across varieties, indicating conserved metabolic dynamics during ripening. While inspecting the functions of the six clusters, we identified metabolites that were enriched in various metabolic and biosynthetic pathways (Fig. 2). These analyses indicated that the metabolic pathways related to flavonoids, glutathione, and pantothenate were weakened at T1, whereas the biosynthesis of anthocyanin, phenylalanine, starch and sucrose increased from T2 to T3. The Sankey diagram illustrates that during the development of kiwifruit, these DAMs were highly accumulated in XZG and QH. Flavonoids were primarily concentrated at T1, followed by T3 and T2 (Fig. S2). These results indicated that metabolite accumulation occurred in a stage-specific manner during the ripening of *A. arguta* fruit. These global patterns provided the basis for subsequent integrative analyses of trait-associated metabolites and regulatory networks.

Transcriptomic changes during kiwifruit ripening

To uncover the potential molecular foundation of metabolism throughout kiwifruit development and ripening, we further performed a comprehensive transcriptomic analysis by constructing 27 cDNA libraries from *A. arguta* using the RNA-seq technique. Each library generated 42.58–49.12 million raw reads and 41.42–47.97 million clean reads (Table S1), with Q30 and GC contents ranging from 93.55–94.52% and 46.25–47.35%, respectively. A variable number of transcripts were identified in *A. arguta* varieties, covering more than 96% (95.84%–97.70%) of the annotated genes in the *A. arguta* 'M' genome (Lu et al. 2024). PCA (Fig. 3a) and hierarchical clustering (Fig. 3b) plots revealed strong correlations among the three biological replicates. In line with the metabolome results, we noticed a clear separation among the different stages and varieties, indicating that the accumulation of metabolites was regulated through differential gene expression. Furthermore, we identified 4545, 9247, and 6248 DEGs that were specifically expressed in the T1 *vs* T3 comparisons of KKW, XZG and QH, respectively. The number of DEGs decreased in subsequent stages, with 2067–2679 genes in the T1 *vs* T2 comparison and 828–1069 genes in the T2 *vs* T3 comparison (Fig. 3c).

A total of 43,468 DEGs (23.34% of all genes) were identified across the three ripening stages, which were grouped into six clusters (C1–C6) (Fig. 4), closely mirroring the metabolite clusters. Among these, 23,347 DEGs (53.71%) in C5 and C6 were predominantly expressed during early fruit development (T1), whereas 10,265 DEGs (23.62%) in C1 and C2 showed higher expression during fruit ripening (T3), particularly in XZG and QH (Fig. 4). Interestingly, the three varieties of *A. arguta* showed consistent expression trends across the six different clusters across the three stages. KEGG enrichment analysis revealed that genes with lowest expression from T2 to T3 (C3 and C4) were primarily involved in carbon fixation in photosynthetic organisms (ko00710), tyrosine metabolism (ko00350), and vitamin B6 metabolism (ko00750). Conversely, the expression of members of C1 tended to increase from T2 to T3, and these genes were enriched in genes involved in galactose metabolism (ko00052), flavonoid biosynthesis (ko00941) and fatty acid metabolism (ko00071), suggesting that these genes may play a positive regulatory role during fruit ripening (Fig. 4). These results suggest that gene expression changes dynamically and closely correspond to the accumulation of major metabolites during different stages of fruit ripening in *A. arguta.*

To further investigate the functions of genes in some critical pathways, we conducted a global test analysis utilizing the quantitative enrichment analysis (QEA) mode of GSEA for DEGs between varieties (Figs. 5, S3). The results of the GSEA indicated that five classical metabolite-associated pathways, namely, flavonoid biosynthesis (ko00941), phenylpropanoid biosynthesis

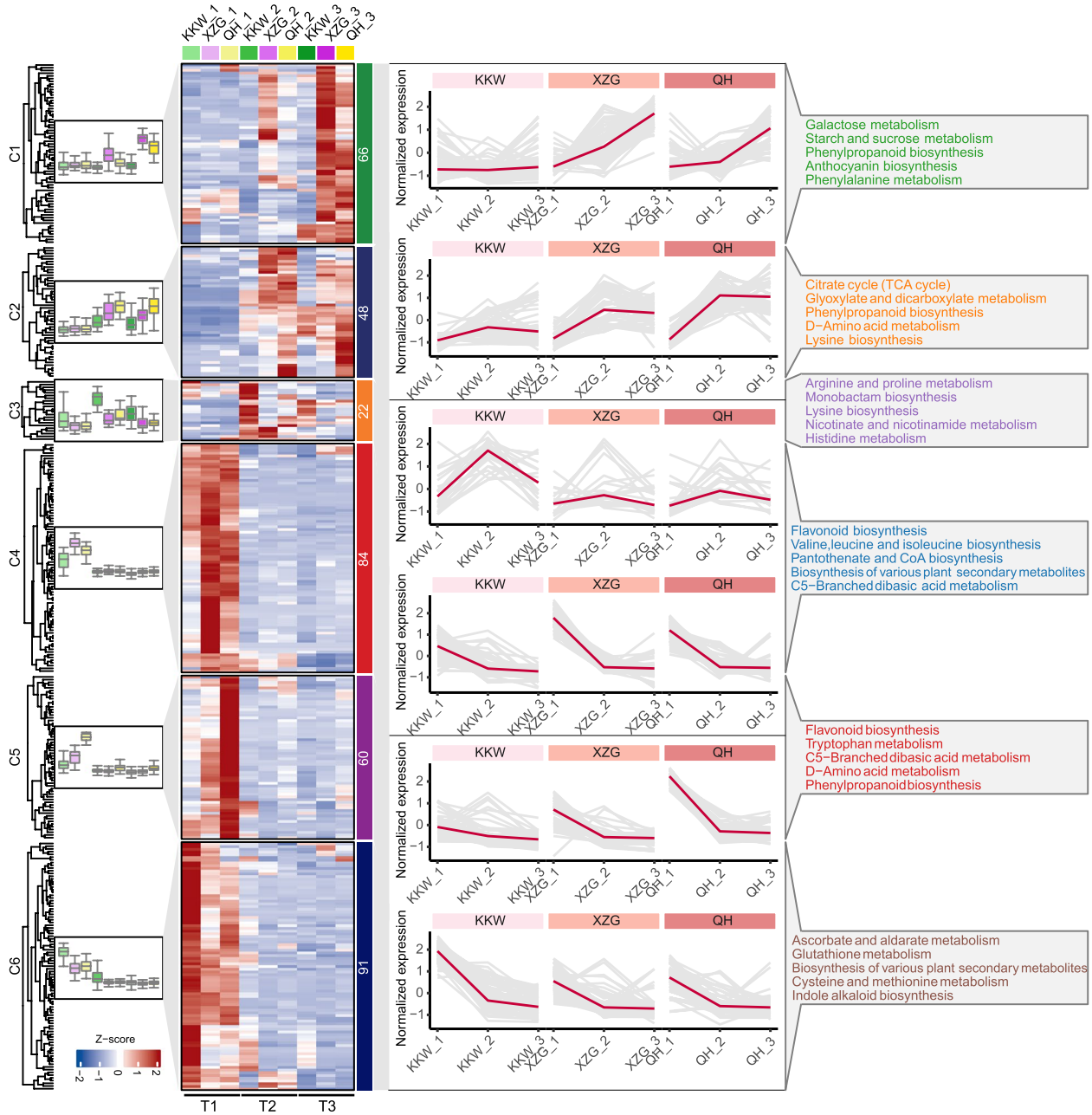


Fig. 2 Metabolic dynamics of *Actinidia arguta* at three ripening stages (T1–T3) based on 371 differentially accumulated metabolites. Each cluster (C1–C6) includes metabolite statistics, heatmaps, clustering analysis, and metabolic pathway enrichment. The gray lines represent the Z scores standardized per metabolite, and the red line indicates the mean trend of all the metabolites. KKW, QH, and XZG represent 'Kokuwa', 'Qinhuang', and 'Xianziguang', respectively

(ko00940), anthocyanin biosynthesis (Ko00942), and starch and sucrose metabolism (ko00500), were enriched in the comparisons of KKW *vs* XZG, KKW *vs* QH and XZG *vs* QH. These findings suggest that these pathways play crucial roles throughout the ripening process of kiwifruit.

Integrative analysis of differentially abundant metabolites and genes

To comprehensively assess kiwifruit quality, we examined the combined contributions of metabolomic and transcriptomic variations to differences in flesh color, taste, and nutritional content among the three varieties. A total of 36 DAMs associated with fruit quality were identified,

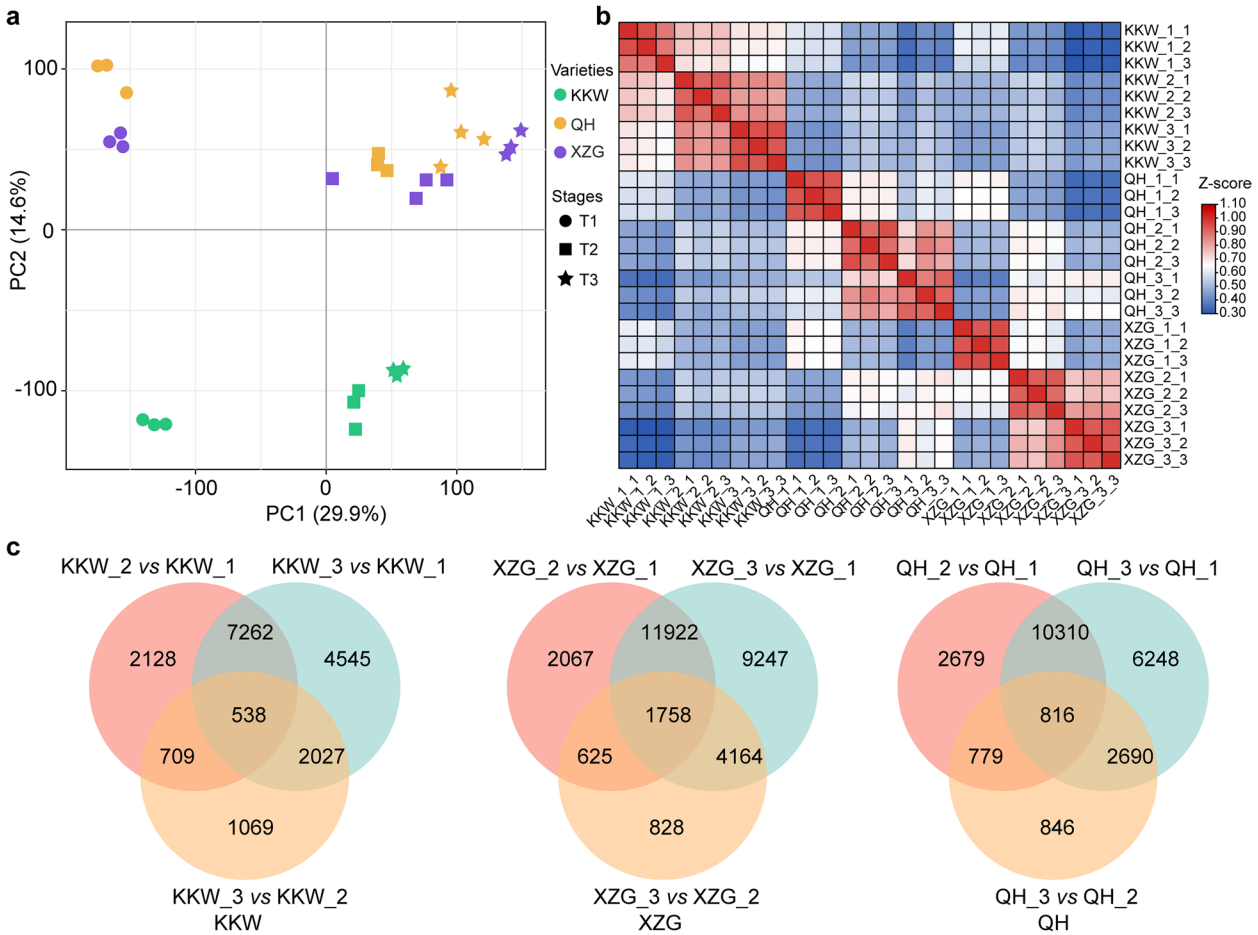


Fig. 3 Global expression profile of *Actinidia arguta* at three ripening stages. **a** Principal component analysis (PCA) of the transcriptome data. **b** Repeated correlation quality of the transcripts. **c** Venn diagram showing the intersection of differentially expressed genes across different comparisons within varieties. KKW, QH, and XZG represent 'Kokuwa', 'Qinhuang', and 'Xianziguang', respectively. T1, T2, and T3 represent kiwifruit samples at the early fruit stage, fruit ripening stage, and fully ripe stage, respectively

including five sugars (e.g., D-glucose and D-sucrose), eight organic acids (e.g., citric acid, isocitric acid, and quinic acid), four volatile or aroma-related compounds (e.g., benzoylformic acid and 4-hydroxybenzaldehyde), thirteen flavonoids (e.g., quercetin-3-O-rutinoside and kaempferol derivatives), one anthocyanin (e.g., cyanidin-3-O-glucoside), and three procyanidins (e.g., procyanidin B2, C1, and B4) involved in anthocyanin/procyanidin biosynthesis (Table S2). These metabolites were designated key DAMs due to their significant differential accumulation across cultivars and established roles in determining sweetness, acidity, pigmentation, and antioxidant capacity. As shown in Fig. S4, the contents of fructose and sucrose tended to increase, whereas the levels of quinic acid, citric acid, and isocitric acid decreased as the fruits ripened. Moreover, we observed that the level of cyanidin-3-o-glucoside dramatically increased at T3, indicating that it may be a characteristic metabolite associated with fruit pulp coloring (Fig. S4). Furthermore, we employed WGCNA to construct a coexpression network and identify the key genes governing fruit quality, providing further insight into the regulation of metabolic changes. In total, 24 distinct coexpression modules were identified on the basis of their similar expression patterns (Fig. S5a). Among these, the MElightpink and MEantiquewhite4 modules were significantly correlated with quality-associated metabolites ($R^2 > 0.80$) (Fig. S5b; Table S3). Specifically, the MElightpink module, composed of 8373 DEGs, was significantly correlated with organic acid ($R^2 > 0.81$) and flavonoid ($R^2 > 0.83$) contents, and the MEantiquewhite4 module, composed of 7,772 DEGs, was preferentially correlated with anthocyanin ($R^2 = 0.85$) and vitamin ($R^2 = 0.81$) accumulation (Fig. S5b).

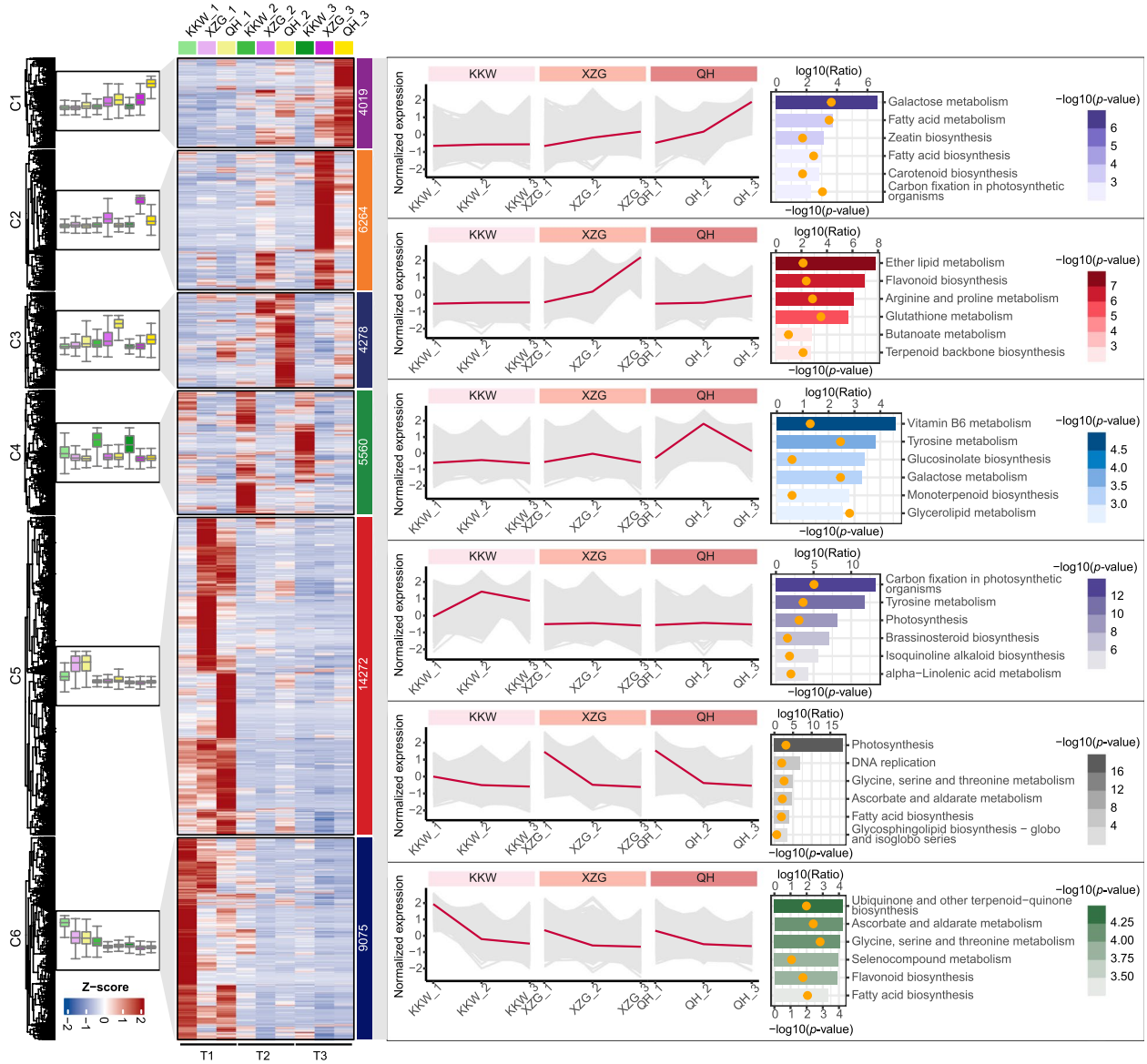


Fig. 4 Transcriptional dynamics of *Actinidia arguta* at three ripening stages (T1–T3) based on 8823 differentially expressed genes. Each cluster (C1–C6) includes gene statistics, heatmaps, clustering analysis, and metabolic pathway enrichment. KKW, QH, and XZG represent 'Kokuwa', 'Qinhuang', and 'Xianziguang', respectively. The gray lines represent the Z score of each standardized gene, and the red line denotes the mean expression trend of all genes. The orange circles represent the enrichment ratios

Dynamics of anthocyanin biosynthesis during *A. arguta* fruit ripening

High anthocyanin content is among the most crucial agricultural traits of *A. arguta*. The growth cycle of the fruit is crucial, as it represents the color transition period from the immature stage to the fully mature stage (T1 to T3), during which anthocyanin biosynthesis plays a central role. In *A. arguta*, anthocyanins are primarily present as cyanidin-3-glucoside, which substantially accumulated in the XZG and QH varieties during the fruit ripening stage (Fig. 6a). Additionally, the metabolic profiles of flavonoids (i.e., chalcones, flavones, flavonols, and proanthocyanidins) exhibited notable dynamics across different varieties and ripening stages. Most flavonoid metabolites, such as kaempferol, quercetin, rutin, and procyanidins, were predominantly abundant at the early developmental stage (T1) and decreased as the fruit matured (Figs. 6a, S6).

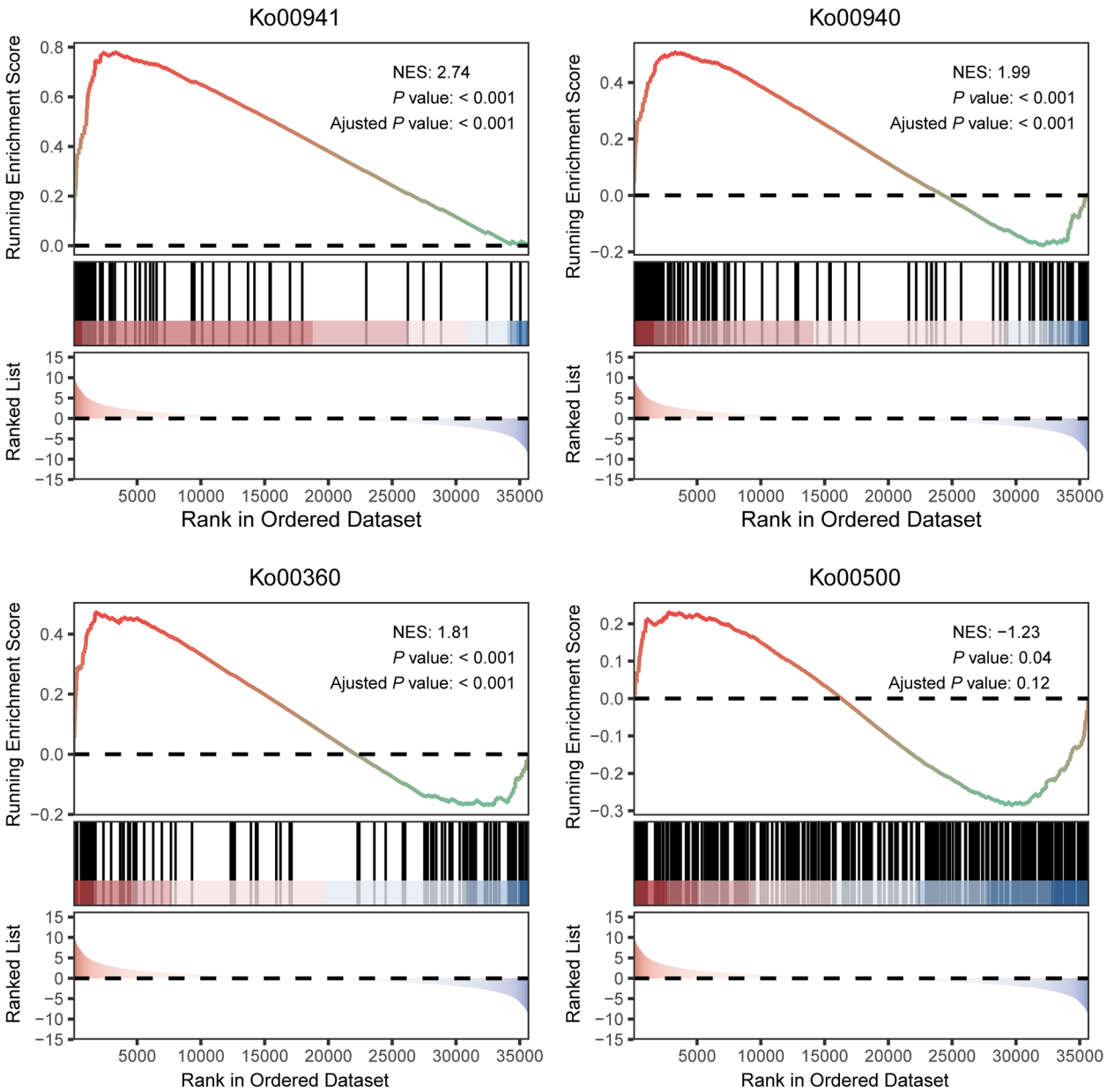


Fig. 5 Gene set enrichment analysis (GSEA) of differentially expressed genes between 'Kokuwa' (KKW) and 'Xianziguang' (XZG). Ko00941, flavonoid biosynthesis; Ko00940, phenylpropanoid biosynthesis; Ko00350, ascorbate and aldarate metabolism; Ko00710, carbon fixation in photosynthetic organisms

The metabolic pathway of flesh coloration was mapped, which included 54 enzymatic genes related to anthocyanin and flavonoid metabolism (Fig. 6a; Table S4). Thirteen important gene families in this pathway were identified, among which the 4-coumarate-CoA ligase (4CL, 10) and transcinnamate 4-monooxygenase (C4H, 6) gene families had many members (Fig. 6a). More specifically, almost all the genes displayed unique expression patterns, with their expression levels varying significantly among the three varieties at different stages. In XZG and QH, genes such as *anthocyanidin synthase* (*ANS*) and *UDP-glycose flavonoid glycosyltransferase* (*UFGT*) were highly expressed at the T3 stage, which aligns with the rapid accumulation of anthocyanins during fruit ripening. Conversely, the expression levels of the *flavonol synthase* (*FLS*), *flavanone 3-hydroxylase* (*F3H*) and *flavonoid 3',5'-hydroxylase* (*F3'5'H*) genes tended to increase during fruit development, with the lowest expression observed at the fruit maturation stage.

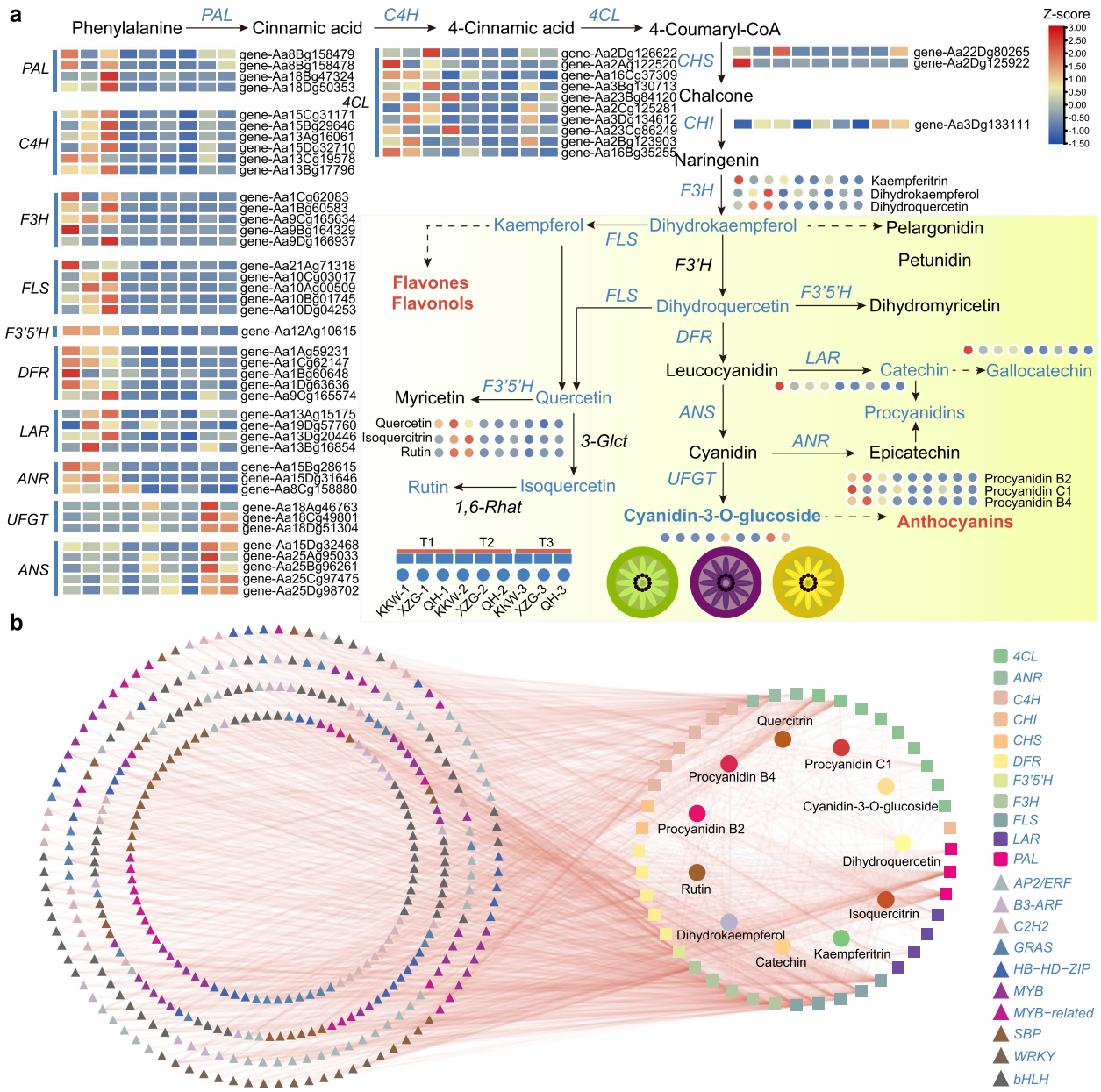


Fig. 6 Reconstruction of anthocyanin biosynthetic pathways during kiwifruit ripening using differentially expressed genes. **a** Expression pattern of anthocyanin biosynthetic genes and identification of related metabolites in *Actinidia arguta* at three developmental stages. KKW, QH, and XZG represent the kiwifruit varieties 'Kokuwa', 'Qinhuang', and 'Xianziguang', respectively. T1, T2, and T3 represent kiwifruit samples at the early fruit stage, fruit ripening stage, and fully ripe stage, respectively. *PAL*, *phenylalanine ammonia-lyase*; *C4H*, *cinnamate 4-hydroxylase*; *4CL*, *4-coumarate-CoA ligase*; *CHS*, *chalcone synthase*; *CHI*, *chalcone isomerase*; *F3H*, *flavanone 3-hydroxylase*; *FLS*, *flavonol synthase*; *F3'H*, *flavonoid 3'-hydroxylase*; *F3'5'H*, *flavonoid 3',5'-hydroxylase*; *DFR*, *dihydro flavonol reductase*; *ANS*, *anthocyanidin synthase*; *UFGT*, *UDP-glycose flavonoid glycosyltransferase*. **b** Coexpression networks of hub genes, TFs, and metabolites involved in flavonoid biosynthesis. Red lines represent the weighted Pearson correlation coefficients between each gene pair

Generation of anthocyanidin regulatory networks

A correlation analysis was conducted using the dataset comprising 54 genes and 17 metabolites throughout the three stages of kiwifruit ripening (Fig. S7; Table S4). Most genes showed positive correlations with flavonoids. Notably, three *UFGT* genes (Aa18Ag46763, Aa18Cg49801, and Aa18Dg51304) and five *ANS* genes (Aa15Dg32468, Aa25Ag95033, Aa25Bg96261, Aa25Cg97475, and Aa25Dg98702) were negatively correlated with the majority of flavonoids and positively

correlated with anthocyanins. Additionally, the *ANR* gene, Aa8Cg158880, demonstrated a strong negative correlation with anthocyanin but was positively correlated with other flavonoids, including flavonols and proanthocyanidins.

To further characterize key TFs associated with anthocyanin accumulation in *A. arguta*, we retrieved a total of 44 hub genes highly correlated with flavonoids ($P < 0.05$) and their upstream regulatory potential TFs in the MElightpink, MEantiquewhite4, MEantiquewhite, and MEolivedrab3 modules to construct an anthocyanin-related regulatory network (Fig. 6b; Tables S3, S4). Classification of the TFs into gene families revealed that AP2/ERF, bHLH, MYB, and C2H2 accounted for 54.96% of the TFs likely governing anthocyanin accumulation (Fig. S8). Notably, *ANR* (Aa15Dg31646 and Aa15Bg28615), *dihydro flavonol reductase* (*DFR*; Aa1Ag59231, Aa1Cg62147, Aa1Bg60648, and Aa1Dg63636), *FLS* (Aa10Ag71318, Aa10Cg03017, Aa10Ag00509, Aa10Bg01745, and Aa10Dg04253), and *phenylalanine ammonia-lyase* (*PAL*; Aa18Bg47324 and Aa18Dg50353) were strongly correlated with multiple TFs, occupying central positions within the network and highlighting the complex regulatory interactions controlling anthocyanin biosynthesis (Fig. 6b). This analysis illustrates the intricate mechanisms regulating anthocyanin accumulation in *A. arguta*, which are critical for fruit development and quality. qRT–PCR analysis confirmed that structural genes, such as *AaANR*, showed significant expression differences among the three varieties (Fig. S9), suggesting that the reduced anthocyanin content in KKW is associated with both the expression of upstream structural genes and the activity of multiple TFs involved in anthocyanin biosynthesis.

Sugars, organic acids and AsA in three *A. arguta* varieties

Sugars and organic acids are key determinants of fruit taste and act as important regulatory signals during kiwifruit ripening. On the basis of the detected metabolites and genes in reference to sucrose and citric acid biosynthesis in the KEGG database, we mapped the central metabolic pathways of associated sugars and organic acids (Fig. 7a). During the fruit ripening process, the levels of six saccharides (sucrose, glucose, lactulose, lactobiose, trehalose 6-phosphate, and melezitose) and four organic acids (citric acid, isocitric acid, l-citramalic acid, and quinic acid) increased significantly, whereas the contents of the other eight acids (e.g., benzoylmalic acid, isopropylmalic acid, and caffeoylquinic acid) significantly decreased (Fig. S6). The expression of genes related to sucrose biosynthesis, including *sucrose synthase* (*SUS*) and *sucrose phosphate synthase* (*SPS*), was high in the three varieties (Fig. 7a; Table S5). Three *SUS* genes (Aa12Bg12382, Aa12Ag11004, and Aa23Cg86846) were more highly expressed in XZG than in KKW and QH. Invertase (INV, EC 3.2.1.26) converts sucrose into glucose and fructose, and the resulting fructose is then phosphorylated to fructose 6-phosphate and glucose 6-phosphate by fructokinase (FK, EC 2.7.1.4) and hexokinase (HK, EC 2.7.1.1), respectively. The expression of *AaFK* was greater in XZG and QH than in KKW during the T1 stage, whereas the expression of *AaHK* was greater than that of *AaFK* during the other stages. To analyze the relationships between sucrose-related DEGs and metabolites, a correlation analysis was further conducted between the 55 DEGs and five metabolites. The analysis revealed the greatest correlation between five *FK* genes (Aa22Bg77653, Aa22Ag76351, Aa22Cg78913, Aa9Dg167142, and Aa3Dg133607) and D-fructose-1,6-bisphosphate, as well as between the *AMY* gene (Aa21Dg74772) and glucose (Fig. S10). The correlation coefficients for the two differentially abundant metabolites (D-glucose and D-fructose-1,6-bisphosphate) with the DEGs were greater than 0.9, whereas a weaker correlation was detected between the other three differentially abundant metabolites (sucrose, trehalose 6-phosphate, and melezitose) and the DEGs (Fig. S10).

Moreover, we identified 23 organic acid-metabolizing genes, including 10 *phosphoenolpyruvate carboxykinase* (pckA), 20 *pyruvate kinase* (*PK*), four *malate dehydrogenase* (*MDH*), and one *isocitrate dehydrogenase* (*IDH*) genes, in the antiquewhite, antiquewhite4 and coral3 modules (Fig. 7a; Tables S3, S5), whose expression was strongly correlated with the accumulation of the three organic acids (Fig. S10). The expression of the citric acid-related genes *AaIDH* and *AapckA* was greater in XZG than in KKW and QH (Fig. 7a). To further characterize the TFs that putatively regulate organic acid metabolism, we screened 184 TFs, including those in the bHLH, MYB, TCP, and bZIP families, in the MEgoldenrod4, MElightpink and MEorange1 modules ($r > 0.9$, $p < 0.05$) and constructed regulatory networks (Fig. 7b). High connectivity between the TFs and genes suggests that these TFs play central roles in controlling sugar and organic acid metabolism during kiwifruit ripening.

AsA is an essential nutritional quality characteristic of kiwifruit. In this study, we explored four key AsA biosynthesis and recycling pathways in kiwifruit: the L-galactose (D-mannose) pathway, the D-galacturonate pathway, the myo-inositol pathway, and the L-gulonate pathway. Two metabolites, L-ascorbate and L-dehydroascorbate, were detected in the AsA biosynthetic pathway (Fig. 7a). We noticed that L-ascorbate accumulation was highest during development in QH but then gradually decreased during subsequent kiwifruit ripening, with a lower content than that in the other two varieties at the T3 stage. In contrast, the accumulation of dehydroascorbic acid

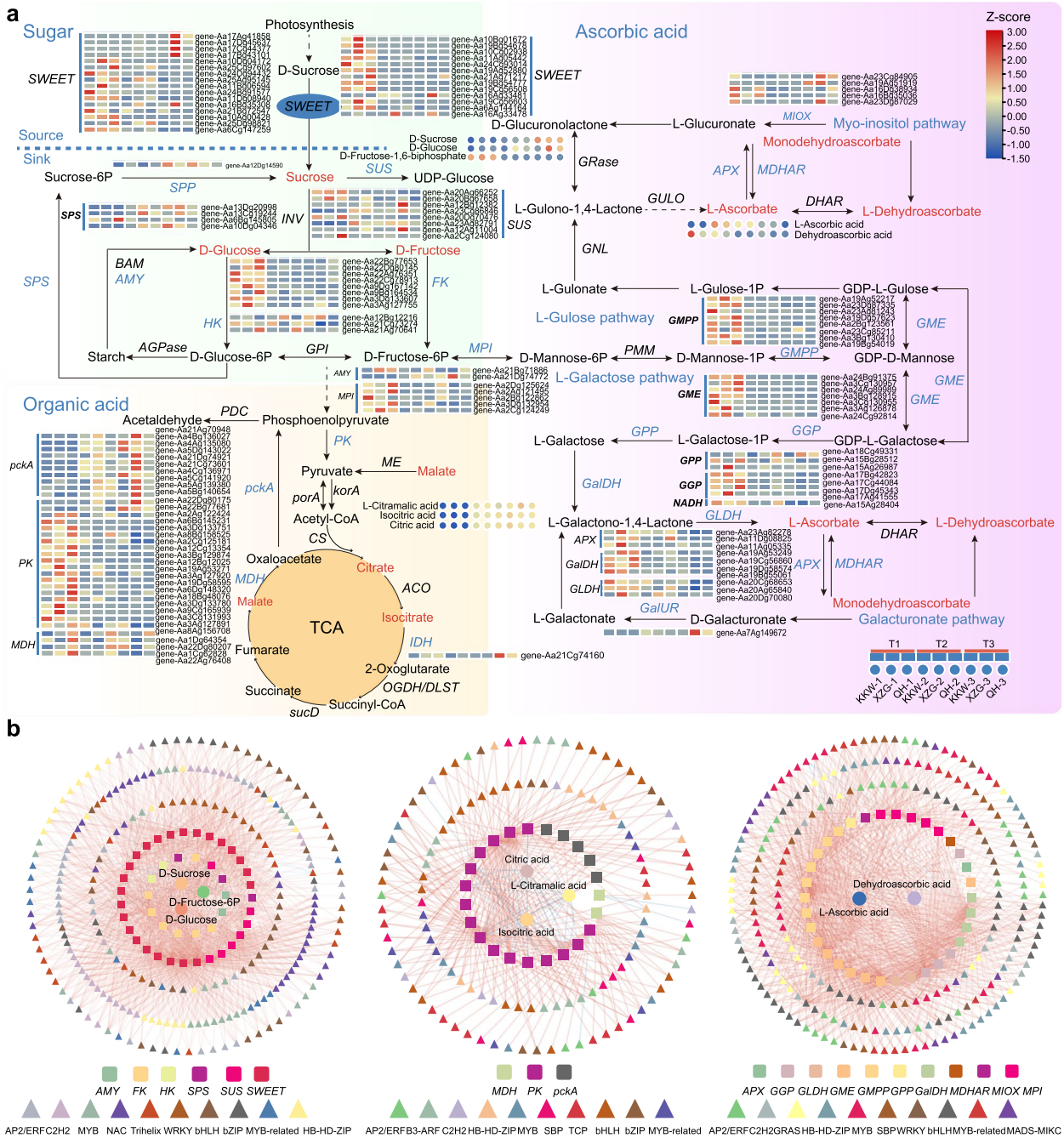


Fig. 7 Reconstruction of sugars, organic acids and L-ascorbic acid (AsA) biosynthetic pathways during kiwifruit ripening using differentially expressed genes. **a** Expression pattern of structural genes and identification of related metabolites involved in sugars, organic acids and AsA in *Actinidia arguta* at three developmental stages. KKW, QH, and XZG represent 'Kukuwa', 'Qinhuang', and 'Xianziguang', respectively. T1, T2, and T3 represent kiwifruit samples at the early fruit stage, fruit ripening stage, and fully ripe stage, respectively. *SWEET*, sugars will eventually be exported transporters; *SUS*, *sucrose synthase*; *SPS*, *sucrose phosphate synthase*; *SPP*, *sucrose-phosphate phosphatase*; *HK*, *hexokinase*; *FK*, *fructokinase*; *AMY*, *a-amylase*; *PK*, *pyruvate kinase*; *IDH*, *isocitrate dehydrogenase*; *MDH*, *malate dehydrogenase*; *pckA*, *phosphoenolpyruvate carboxykinase* (ATP); *ME*, *malate enzyme*; *CS*, *citrate synthase*; *ACO*, *aconitase*; *MIOX*, *inositol oxygenase*; *MPI*, *mannose-6-phosphate isomerase*; *NADH*, *monodehydroascorbate reductase*; *OGDH*, *2-oxoglutarate dehydrogenase E1 component*; *APX*, *L-ascorbate peroxidase*; *GalDH*, *L-galactose dehydrogenase*; *GalUR*, *D-galacturonate reductase*; *GGP*, *GDP-L-galactose phosphorylase*; *GLD*, *L-galactono-1,4-lactone dehydrogenase*; *GME*, *GDP-D-mannose 3', 5'-epimerase*; *GMPP*, *mannose-1-phosphate guanylyltransferase*; *GPP*, *inositol-phosphate phosphatase/L-galactose 1-phosphate phosphatase*. **b** Coexpression networks of genes, TFs, and metabolites involved in sugars, organic acids, and AsA biosynthesis, respectively. Red lines indicate the weighted Pearson correlation coefficient values for each gene pair

(DHA) and the expression of AsA biosynthetic genes, including *L-galactose dehydrogenase* (*GalDH*), *GDP-L-galactose phosphorylase* (*GGP*), *GDP-D-mannose 3,5'-epimerase* (*GME*), and *mannose-1-phosphate guanylyltransferase* (*GMPP*), were found to display consistent patterns at different ripening stages. Notably, DHA accumulated the most in XZG and QH, which was consistent with the peak expression of *D-galacturonate reductase* (*GalUR*), *inositol-phosphate phosphatase/L-galactose 1-phosphate* (*GPP*), and *inositol oxygenase* (*MIOX*) during the ripening stage (Fig. 7a). This dynamic expression pattern suggests that these genes might be involved in the response to fruit ripening. To verify the accuracy of the screened genes, we selected six DEGs (*AaAPX1*, *AaAPX2*, *AaAPX3*, *AaSWEET1*, *AaSWEET2*, and *AaANR*) for qRT–PCR analysis (Fig. S9).

To reconstruct AsA metabolic regulatory networks, we initially examined 34 critical genes, including *GalDH*, *GPP*, *GME*, and *GMPP*, whose expression was strongly correlated (Figs. 7b, S10). Additionally, 343 potential TFs, e.g., AP2/ERF, bHLH, MYB and WRKY, were identified and strongly correlated ($r > 0.90$) with the AsA metabolic profile. Among the 343 TFs in the correlation network, 63 corresponded to bHLH-type TFs (Fig. S8), highlighting the significant role of the bHLH family in modulating AsA biosynthesis.

Discussion

Kiwifruit varieties are highly diverse in terms of appearance and taste and contain abundant functional compounds, which have been demonstrated to possess many exceptional physiological activities (Richardson et al. 2018; Wang et al. 2021a, b). Although advanced metabolomics technologies have identified many compounds associated with kiwifruit quality, understanding of the physiological and molecular mechanisms governing fruit ripening remains limited. Determining the metabolic pathways of key compounds and their underlying regulatory networks in diverse kiwifruit varieties is critical for improving fruit quality via genetic improvement. In this study, we integrated metabolomic and transcriptomic analyses of 27 fruit samples that represent the major growth stages of three *A. arguta* varieties exhibiting different colors. Global analyses revealed that 371 metabolites and 43,468 genes could be clustered into six distinct modules, highlighting clear stage-specific patterns during fruit development. Many identified metabolites exhibited significant developmental specificity at different developmental stages of the three varieties, especially the DAMs enriched in sugars, organic acids and other nutritional components at the ripening stage. Consistent with the results of the metabolomic patterns, the results of the transcriptomic analysis revealed three distinct transitions from T1 to T2 and T2 to T3, suggesting that three different physiological processes occur from the fruitlet stage to the middle and late stages of fruit ripening. Overall, stage specificity was evident from both metabolite profiles and transcriptional changes, aligning with observations in other fruits such as citrus (Zhu et al. 2024), mango (Wu et al. 2022), and watermelon (Umer et al. 2020). Using our dataset, we dissected several kiwifruit quality-related metabolic regulatory networks and identified key structural genes and TFs that coordinate the accumulation of sugars, organic acids, AsA, and anthocyanins.

Anthocyanin, an essential bioactive metabolite in the human diet, is associated with a dynamic and close relationship between its content and fruit color variation (Jaakola 2013; Liu et al. 2017; Meng et al. 2020). Our study demonstrated that the key dynamic change during the ripening process of red XZG and yellow QH is the increase in cyanidin-3-o-glucoside levels, whereas in KKW, cyanidin levels decreased from T1 to T2 and T3. Cyanidin-based anthocyanins have previously been detected in *A. chinensis*, *A. melanandra*, and *A. arguta* var. *purpurea* (Montefiori et al. 2011; Peng et al. 2020). A comparison of the transcription of anthocyanin biosynthetic genes among the three *A. arguta* varieties revealed a strong correlation between the expression of *AaANS* and *AaUFGT* and the accumulation of cyanidin-3-o-glucoside. Similarly, compared with that in KW, the expression of *AaANS* and *AaUFGT* in XZG and QH significantly increased during the ripening stage. Previous studies have confirmed that *ANS* and *UFGT* are responsible for anthocyanin biosynthesis in other fruit crops (Gouot et al. 2019). Conversely, the expression of most biosynthetic genes, especially *AaANR*, *AaDFR*, and *AaF3'5'H*, significantly increased during the early stages of fruit development. These genes exhibited a significant positive correlation with proanthocyanidin levels, but no statistically significant association was observed between their expression and anthocyanin accumulation. The high expression levels of the middle and downstream genes implied an increased influx of the phenylpropanoid pathway, ensuring the production of naringenin and offering sufficient precursor compounds for the biosynthesis of flavonoids and anthocyanins. These observations are consistent with those of previous studies on grapes (Lu et al. 2021) and watermelon (Chu et al. 2022), in which the direct correlation between modifying enzymes and final products contributed to fruit color formation, further supporting the transcriptional mechanism of kiwifruit variety-specific color. Notably, carotenoid-related pigmentation in QH was not captured by our broadly targeted LC–MS/MS platform, and the transcriptomic data did not clearly reveal differential expression of

carotenoid- or chlorophyll-related genes among the three varieties. The limited availability of standard compounds for secondary metabolites restricts comprehensive metabolic coverage (Dumont et al. 2020), and nonpolar compounds such as carotenoids were not quantified in this study. Therefore, the results of the present analysis primarily reflect anthocyanin-driven color variation, and additional targeted carotenoid profiling is needed to fully explain the yellow flesh of QH.

Furthermore, we identified four coexpression modules that were strongly correlated with flavonoid variation. High numbers of TFs belonging to the AP2/ERF, bHLH, MYB and C2H2 families were found in the coexpression regulatory network, indicating that these TFs may regulate flavonoid biosynthetic genes. Notably, the bHLH family is among the largest TF families in plants. Specifically, bHLH IIIf-type TFs have been identified as key regulators that activate anthocyanin biosynthesis in various fruits, such as apple (Xie et al. 2012), bilberry (Samkumar et al. 2021), and strawberry (Li et al. 2020a). In addition, *AabHLH42* has been suggested to regulate anthocyanin biosynthesis by interacting with *AaMYBC1* in *A. arguta* (Li et al. 2020b). In this study, three bHLH members (Aa25Bg96110, Aa5Ag139151, and Aa21Dg74953) homologous to *VvbHLH71* from *Vitis vinifera* were found to be positively correlated with *AaANR* expression, suggesting their potential roles in anthocyanin biosynthesis. The greatest number of MYB TFs (including MYB-related TFs) was found in the coexpression network. These can be classified into 1R-, R2R3-, 3R-, and 4R-MYB subfamilies on the basis of conserved DNA-binding domains (Li et al. 2019a, b). Certain MYB members interact with bHLH TFs to form transcriptional complexes that coordinately activate downstream structural genes. A representative example is the AcMYBF110-AcbHLH1-AcWDR1 complex in *A. chinensis*, which modulates anthocyanin accumulation (Liu et al. 2021). Through the coexpression network, we also revealed other uncharacterized TFs that may act as potential regulators of flavonoid biosynthesis. These findings were consistent with the earlier assertion that flesh color may be genetically regulated by complex networks (Hermanns et al. 2020; Chu et al. 2022).

In general, fruit taste is primarily determined by the composition of soluble sugars and organic acids and the ratio of sugars to organic acids, whereas flavonoids and vitamins with antioxidant activities substantially contribute to human nutrition (Wang et al. 2021a, b; Shu et al. 2023). Our RNA-seq analysis revealed extensive transcriptional changes in genes involved in the sugar, organic acid, and AsA biosynthetic pathways, which strongly correlated with the dynamic changes observed in the metabolite profiles. For instance, the expression of members of the SWEET family, which are known to encode sugar transporters that facilitate sugar translocation and accumulation (Chen et al. 2012), significantly positively correlated with D-glucose and D-fructose-1,6-bisphosphate levels. These findings suggest that SWEET transporters might play a crucial role in regulating sugar levels during kiwifruit ripening, similar to their known function in many fruit crops, such as apple (Li et al. 2012) and watermelon (Umer et al. 2020). Additionally, the coordinated shifts in sugars and organic acids indicate stage-specific metabolic transitions, supported by the elevated expression of *AaSPS* and *sucrose-phosphate phosphatase* (*AaSPP*), together with increased *AaIDH* and *AapckA* activity at the full-ripe stage across the three kiwifruit varieties. These ripening-associated patterns are broadly consistent with findings in *A. chinensis* and *A. eriantha* (Liao et al. 2022; Shu et al. 2023). Notably, the glucose levels in 4×XZG and QH were consistently higher than those in 8×KKW across the three different stages, whereas the other metabolites did not significantly differ in terms of ploidy. These findings indicate that the accumulation of key metabolites is not strictly correlated with ploidy level, which is consistent with previous findings in *A. arguta* (Zhang et al. 2019). Moreover, the expression patterns of *AaGME*, *AaGalDH*, and *AaGMPP* were consistent across the different varieties and positively correlated with the DHA content, similar to the results reported for *A. deliciosa* cv. 'Qinmei', *A. eriantha* and *A. latifolia* (Li et al. 2010; Liao et al. 2019; Deng et al. 2022). The enrichment of bHLH-type TFs (63/343) highlights this family as a central regulator of AsA biosynthesis, which is consistent with their reported roles in coordinating diverse metabolic branches (Ye et al. 2019; Zhao et al. 2023). Future studies are required to clarify ascorbate metabolism and the regulatory network underlying vitamin C accumulation in kiwifruit.

Conclusions

In summary, we constructed a temporal map of the metabolomes and transcriptomes of three kiwifruit varieties with distinct flesh colors during ripening. This study elucidates the transcriptional regulatory networks governing key metabolites, including sucrose, citric acid, anthocyanins/proanthocyanidins, and AsA, providing insights into metabolic dynamics and offering valuable genetic information to guide the improvement of kiwifruit quality.

Supplementary Information

The online version contains supplementary material available at https://doi.org/10.1007/s44281-026-00107-9.

Supplementary Material 1: Figure S1. Pie chart of primary metabolites identified in *Actinidia arguta*.

Supplementary Material 2: Figure S2. Sankey diagram of metabolite compound changes during kiwifruit ripening. KKW, QH, and XZG represent the kiwifruit varieties 'Kokuwa','Qinhuang', and 'Xianziguang', respectively. T1, T2, and T3 represent kiwifruit samples at the early fruit stage, fruit ripening stage, and fully ripe stage, respectively.

Supplementary Material 3: Figure S3. GSEA enrichment analysis of differentially expressed genes (DEGs) between KKW *vs* QH (a) and XZG *vs* QH (b). Ko00940, phenylpropanoid biosynthesis; Ko00941, flavonoid biosynthesis; Ko00942, anthocyanin biosynthesis; Ko00040, pentose and glucuronate interconversions; Ko00052, galactose metabolism; Ko00480, glutathione metabolism; Ko00500, starch and sucrose metabolism.

Supplementary Material 4: Figure S4. Dynamic changes in key metabolites related to sugars, organic acids, and anthocyanins.

Supplementary Material 5: Figure S5. Transcriptomic and metabolic correlation analysis across different stages of *A. arguta* varieties. a Dendrogram showing coexpression modules (clusters) identified by WGCNA across different stages of kiwifruit development. b Relationships between gene coexpression modules and the content of differentially accumulated metabolites (DAMs) involved in fruit quality. The numbers in each cell represent a correlation coefficient and a *P* value (in parentheses).

Supplementary Material 6: Figure S6. Heatmap of differentially accumulated metabolites involved in fruit quality.

Supplementary Material 7: Figure S7. Correlation between hub gene expression and the concentration of flavonoid metabolites. *PAL*, *phenylalanine ammonia-lyase*; *LAR*, *leucoanthocyanidin reductase*; *C4H*,*cinnamate 4-hydroxylase*; *4CL*, *4-coumarate-CoA ligase*; *CHS*,*chalcone synthase*; *CHI*, *chalcone isomerase*; *F3H*, *flavanone 3-hydroxylase*; *FLS*, *flavonol synthase*; *F3′H*, *flavonoid 3′-hydroxylase*; *F3′5′H*, *flavonoid 3′,5′-hydroxylase*; *DFR*, *dihydroflavonol reductase*; *ANS*, *anthocyanidin synthase, ANR*, *anthocyanidin reductase*; *UFGT*, *UDP-glycose flavonoid glycosyltransferase*.

Supplementary Material 8: Figure S8. Statistical analysis of the top 10 transcription factor families in the regulatory networks of flavonoids, sugars, and organic acids within the WGCNA models.

Supplementary Material 9: Figure S9. Validation and expression analysis of selected genes using qRT–PCR ($^{*}P< 0.05$, $^{**}P < 0.01$, and $^{***}P < 0.001$) in *A. arguta* fruits. *APX*, *L-ascorbate peroxidase 1*.

Supplementary Material 10: Figure S10. Correlation between hub gene expression and concentrations of sugars, organic acids, and ascorbic acid. *SWEET*, sugars will eventually be exported transporters; *SUS*, *sucrose synthase*; *SPS*,*sucrose phosphate synthase*; *SPP*, *sucrose-phosphate phosphatase*;*HK*, *hexokinase*; *FK*, *fructokinase*; *AMY*, *α-amylase*;*PK*, *pyruvate kinase*; *IDH*, *isocitrate dehydrogenase*;*MDH*, *malate dehydrogenase*; *pckA*, *phosphoenolpyruvate carboxykinase*; *MIOX*, *inositol oxygenase*; *MPI*, *mannose-6-phosphate isomerase*; *MDHAR*, *monodehydroascorbate reductase*; *APX*,*L-ascorbate peroxidase*; *GalDH*, *L-galactose dehydrogenase*; *GalUR*,*D-galacturonate reductase*; *GGP*, *GDP-L-galactose phosphorylase*;*GLDH*, *L-galactono-1,4-lactone dehydrogenase*; *GME*, *GDP-D-mannose 3′, 5′-epimerase*; *GMPP*, *mannose-1-phosphate guanylyltransferase*;*GPP*, *inositol-phosphate phosphatase/L-galactose 1-phosphate phosphatase*.

Supplementary Material 11: Table S1. Overview of the transcriptome sequencing dataset and quality check. Table S2. Representative differentially accumulated metabolites involved in kiwifruit quality. Table S3. List of modules of interest within metabolite-based modules. Table S4. Differentially expressed structural genes involved in flavonoid biosynthesis. Table S5. Differentially expressed structural genes associated with sugars, organic acids, and ascorbic acid.

Acknowledgements
Not applicable.

Authors' contributions
YZ, YJ and FBD designed the study; YZ, YJ, FBD, LZ, FWW, YPW, YZ, and YLW undertook field research and sampling; YJ, XQ, MW, and TR conducted the data analysis; YCW provided the reference genome data resources that supported this study; YJ and YZ wrote and edited the manuscript. All authors read and approved the final manuscript.

Funding
This work was financially supported by the National Natural Science Foundation of China (32300314), the Shaanxi Academy of Sciences Project (2022 K-09, 2019 k-01(2021)), Xi'an Botanical Garden of Shaanxi Province Young Talent Funding Project (2024TJ-02), the Science and Technology Department of Shaanxi Province Project (2023-JC-QN-0253), and Xi'an Bureau of Science and Technology Project (23NYGG0030, 24NYGG0067).

Data availability
Data supporting the findings are available in the article and supplementary information.

Declarations

Ethics approval and consent to participate
Not applicable.

Consent for publication
Not applicable.

Competing interests
The authors declare that they have no competing interests.

Received: 18 September 2025 Revised: 3 February 2026 Accepted: 6 February 2026
Published online: 20 June 2026

References

Ampomah-Dwamena C, McGhie T, Reginald W, Montefiori M, Hellens RP, Allan AC. The kiwifruit lycopene beta-cyclase plays a significant role in carotenoid accumulation in fruit. J Exp Bot. 2009;60:3765–79. https://doi.org/10.1093/jxb/erp218.

Chen LQ, Hou BH, Lalonde S, Takanaga H, Hartung ML, Qu XQ, et al. Sugar transporters for intercellular exchange and nutrition of pathogens. Nature. 2012;468:527–32. https://doi.org/10.1038/nature09606.

Chen S, Zhou Y, Chen Y, Gu J. Fastp: an ultra-fast all-in-one FASTQ preprocessor. Bioinformatics. 2018;34:i884–90. https://doi.org/10.1093/bioinformatics/bty560.

Chen T, Qin G, Tian S. Regulatory network of fruit ripening: current understanding and future challenges. New Phytol. 2020;228:1219–26. https://doi.org/10.1111/nph.16822.

Chen Y, Shu P, Wang R, Du X, Xie Y, Du K, et al. Ethylene response factor AcERF91 affects ascorbate metabolism via regulation of GDP-galactose phosphorylase encoding gene (*AcGGP3*) in kiwifruit. Plant Sci. 2021;313:111063. https://doi.org/10.1016/j.plantsci.2021.111063.

Chu S, Wang S, Zhang R, Yin M, Yang X, Shi Q. Integrative analysis of transcriptomic and metabolomic profiles reveals new insights into the molecular foundation of fruit quality formation in *Citrullus lanatus* (Thunb.) Matsum. & Nakai. Food Qual Saf. 2022;6:fyac015. https://doi.org/10.1093/fqsafe/fyac015.

Deng H, Xia H, Guo Y, Liu X, Lin L, Wang J, et al. Dynamic changes in ascorbic acid content during fruit development and ripening of *Actinidia latifolia* (an ascorbate-rich fruit crop) and the associated molecular mechanisms. Int J Mol Sci. 2022;23:5808. https://doi.org/10.3390/ijms23105808.

Dias M, Caleja C, Pereira C, Calhelha RC, Kostic M, Sokovic M, et al. Chemical composition and bioactive properties of byproducts from two different kiwi varieties. Food Res Int. 2020;127:108753. https://doi.org/10.1016/j.foodres.2019.108753.

Dumont D, Danielato G, Chastellier A, Hibrand Saint Oyant L, Fanciullino AL, Lugan R. Multi-targeted metabolic profiling of carotenoids, phenolic compounds and primary metabolites in Goji (*Lycium spp.*) berry and tomato (*Solanum lycopersicum*) reveals inter and intra genus biomarkers. Metabolites. 2020;10:422. https://doi.org/10.3390/metabo10100422.

Gouot JC, Smith JP, Holzapfel BP, Walker AR, Barril C. Grape berry flavonoids: a review of their biochemical responses to high and extreme high temperatures. J Exp Bot. 2019;70:397–423. https://doi.org/10.1093/jxb/ery392.

Gu Z, Eils R, Schlesner M. Complex heatmaps reveal patterns and correlations in multidimensional genomic data. Bioinformatics. 2016;32:2847–9. https://doi.org/10.1093/bioinformatics/btw313.

Hermanns AS, Zhou X, Xu Q, Tadmor Y, Li L. Carotenoid pigment accumulation in horticultural plants. Hortic Plant J. 2020;6:343–60. https://doi.org/10.1016/j.hpj.2020.10.002.

Hou YF, Bai L, Guo S, Hu JB, Zhang SS, Liu SJ, et al. Nontargeted metabolomic analysis of four different parts of *Actinidia arguta* by UPLC-Q-TOF-MS^{E}. Food Res Int. 2023;163:112228. https://doi.org/10.1016/j.foodres.2022.112228.

Huang S, Ding J, Deng D, Tang W, Sun H, Liu D, et al. Draft genome of the kiwifruit *Actinidia chinensis*. Nat Commun. 2013;4:2640. https://doi.org/10.1038/ncomms3640.

Jaakola L. New insights into the regulation of anthocyanin biosynthesis in fruits. Trends Plant Sci. 2013;18:477–83. https://doi.org/10.1016/j.tplants.2013.06.003.

Jia Y, Zhang Y, Zhang L, Wang F, Yu G, Wang Y, et al. Characterization and analysis of the full-length transcriptome provide insights into fruit quality formation in kiwifruit cultivar *Actinidia arguta* cv. Qinziyu. Agronomy. 2023;13:143. https://doi.org/10.3390/agronomy13010143.

Kataoka I, Mizugami T, Kim JG, Beppu K, Fukuda T, Sugahara S, et al. Ploidy variation of hardy kiwifruit (*Actinidia arguta*) resources and geographic distribution in Japan. Sci Hortic. 2010;124:409–14. https://doi.org/10.1016/j.scienta.2010.01.016.

Kim D, Langmead B, Salzberg SL. HISAT: a fast spliced aligner with low memory requirements. Nat Methods. 2015;12:357–60. https://doi.org/10.1038/nmeth.3317.

Kohl M, Wiese S, Warscheid B. CYTOSCAPE: software for visualization and analysis of biological networks. Methods Mol Biol. 2011;696:291–303. https://doi.org/10.1007/978-1-60761-987-1_18.

Langfelder P, Horvath S. WGCNA: an R package for weighted correlation network analysis. BMC Bioinformatics. 2008;9:559. https://doi.org/10.1186/1471-2105-9-559.

Li J, Han G, Sun C, Sui N. Research advances of MYB transcription factors in plant stress resistance and breeding. Plant Signal Behav. 2019a;14:1613131. https://doi.org/10.1080/15592324.2019.1613131.

Li M, Feng F, Cheng L. Expression patterns of genes involved in sugar metabolism and accumulation during apple fruit development. PLoS ONE. 2012;7:e33055. https://doi.org/10.1371/journal.pone.0033055.

Li M, Ma F, Liang D, Li J, Wang Y. Ascorbate biosynthesis during early fruit development is the main reason for its accumulation in kiwi. PLoS ONE. 2010;5:e14281. https://doi.org/10.1371/journal.pone.0014281.

Li Y, Fang J, Qi X, Lin M, Zhong Y, Sun L, et al. Combined analysis of the fruit metabolome and transcriptome reveals candidate genes involved in flavonoid biosynthesis in *Actinidia arguta*. Int J Mol Sci. 2018;19:1471. https://doi.org/10.3390/ijms19051471.

Li Y, Song Z, Zhan X, Lin M, Li X, Wang R, et al. AaEIL2 and AaERF059 are involved in fruit coloration and ripening by crossly regulating ethylene and auxin signal pathway in *Actinidia arguta*. Hortic Plant J. 2025. https://doi.org/10.1016/j.hpj.2024.07.013.

Li Y, Xu P, Chen G, Wu J, Liu Z, Lian H. FvbHLH9 functions as a positive regulator of anthocyanin biosynthesis by forming a HY5-bHLH9 transcription complex in strawberry fruits. Plant Cell Physiol. 2020a;61:826–37. https://doi.org/10.1093/pcp/pcaa010.

Li Y, Cui W, Qi X, Lin M, Qiao C, Zhong Y, et al. MicroRNA858 negatively regulates anthocyanin biosynthesis by repressing *AaMYBC1* expression in kiwifruit (*Actinidia arguta*). Plant Sci. 2020b;296:110476. https://doi.org/10.1016/j.plantsci.2020.110476.

Li Y, Cui W, Wang R, Lin M, Zhong Y, Sun L, et al. MicroRNA858-mediated regulation of anthocyanin biosynthesis in kiwifruit (*Actinidia arguta*) based on small RNA sequencing. PLoS ONE. 2019b;14:e0217480. https://doi.org/10.1371/journal.pone.0217480.

Liao G, Li Y, Wang H, Liu Q, Zhong M, Jia D, et al. Genome-wide identification and expression profiling analysis of sucrose synthase (SUS) and sucrose phosphate synthase (SPS) genes family in *Actinidia chinensis* and *A. eriantha*. BMC Plant Biol. 2022;22:215. https://doi.org/10.1186/s12870-022-03603-y.

Liao G, He Y, Li X, Zhong M, Huang C, Yi S, et al. Effects of bagging on fruit flavor quality and related gene expression of AsA synthesis in *Actinidia eriantha*. Sci Hortic. 2019;256:108511. https://doi.org/10.1016/j.scienta.2019.05.038.

Lin Y, Tang H, Zhao B, Lei D, Zhou X, Yao W, et al. Comparative changes of health-promoting phytochemicals and sugar metabolism of two hardy kiwifruit (*Actinidia arguta*) cultivars during fruit development and maturity. Front Plant Sci. 2022;13:1087452. https://doi.org/10.3389/fpls.2022.1087452.

Liu X, Wu R, Bulley SM, Zhong C, Li D. Kiwifruit MYBS1-like and GBF3 transcription factors influence L-ascorbic acid biosynthesis by activating transcription of *GDP-L-galactose phosphorylase 3*. New Phytol. 2022;234:1782. https://doi.org/10.1111/nph.18097.

Liu Y, Ma K, Qi Y, Lv G, Ren X, Liu Z, et al. Transcriptional regulation of anthocyanin synthesis by MYB-bHLH-WDR complexes in kiwifruit *Actinidia chinensis*. J Agric Food Chem. 2021;69:3677–91. https://doi.org/10.1021/acs.jafc.0c07037.

Liu Y, Zhou B, Qi Y, Chen X, Liu C, Liu Z, et al. Expression differences of pigment structural genes and transcription factors explain flesh coloration in three contrasting kiwifruit cultivars. Front Plant Sci. 2017;8:1507. https://doi.org/10.3389/fpls.2017.01507.

Lu S, Wang J, Zhuge Y, Zhang M, Liu C, Jia H, et al. Integrative analyses of metabolomes and transcriptomes provide insights into flavonoid variation in grape berries. J Agric Food Chem. 2021;69:12354–67. https://doi.org/10.1021/acs.jafc.1c02703.

Lu X, Man Y, Lei R, Liu Y, Wu J, Wang Y. Structural analysis of *Actinidia arguta* natural populations and preliminary application in association mapping of fruit traits. Sci Hortic. 2022;304:111306. https://doi.org/10.1016/j.scienta.2022.111306.

Lu X, Yu X, Li G, Qu M, Wang H, Liu C, et al. Genome assembly of autotetraploid *Actinidia arguta* highlights adaptive evolution and enables dissection of important economic traits. Plant Commun. 2024;5:100856. https://doi.org/10.1016/j.xplc.2024.100856.

Meng J, Gao Y, Han M, Liu P, Yang C, Shen T, et al. *In vitro* anthocyanin induction and metabolite analysis in *Malus spectabilis* leaves under low nitrogen conditions. Hortic Plant J. 2020;6:284–92. https://doi.org/10.1016/j.hpj.2020.06.004.

Montefiori M, Espley RV, Stevenson D, Cooney J, Datson PM, Saiz A, et al. Identification and characterisation of F3GT1 and F3GGT1, two glycosyltransferases responsible for anthocyanin biosynthesis in red-fleshed kiwifruit (*Actinidia chinensis*). Plant J. 2011;65:106–18. https://doi.org/10.1111/j.1365-313X.2010.04409.x.

Nardozza S, Boldingh HL, Kashuba MP, Feil R, Jones D, Thrimawithana AH, et al. Carbon starvation reduces carbohydrate and anthocyanin accumulation in red-fleshed fruit via trehalose 6-phosphate and MYB27. Plant Cell Environ. 2020;43:819–35. https://doi.org/10.1111/pce.13699.

Peng Y, Thrimawithana AH, Cooney JM, Jensen DJ, Espley RV, Allan AC. The proanthocyanin-related transcription factors MYBC1 and WRKY44 regulate branch points in the kiwifruit anthocyanin pathway. Sci Rep. 2020;10:14161. https://doi.org/10.1038/s41598-020-70977-0.

Pérez-Burillo S, Oliveras MJ, Quesada J, Rufián-Henares JA, Pastoriza S. Relationship between composition and bioactivity of persimmon and kiwifruit. Food Res Int. 2018;105:461–72. https://doi.org/10.1016/j.foodres.2017.11.022.

Popowski E, Thomson SJ, Knäbel M, Tahir J, Crowhurst RN, Davy M, et al. Construction of a high-density genetic map for hexaploid kiwifruit (*Actinidia chinensis* var. *deliciosa*) using genotyping by sequencing. G3 Bethesda. 2021;11:jkab142. https://doi.org/10.1093/g3journal/jkab142.

Putri GH, Anders S, Pyl PT, Pimanda JE, Zanini F. Analysing high-throughput sequencing data in Python with HTSeq 2.0. Bioinformatics. 2022;38:2943–5. https://doi.org/10.1093/bioinformatics/btac166.

Qiang X, Ren T, Zhang Y, Jia Y. Genome-wide identification and expression profiling of the invertase genes involved in sugar metabolism and accumulation in *Actinidia arguta*. Int J Mol Sci. 2025;26:2150. https://doi.org/10.3390/ijms26052150.
R Core Team. R: A language and environment for statistical computing. Vienna, Austria: R Foundation for Statistical Computing; 2023.
Richardson DP, Ansell J, Drummond LN. The nutritional and health attributes of kiwifruit: a review. Eur J Nutr. 2018;57:2659–76. https://doi.org/10.1007/s00394-018-1627-z.
Samkumar A, Jones D, Karppinen K, Dare AP, Sipari N, Espley RV, et al. Red and blue light treatments of ripening bilberry fruits reveal differences in signalling through abscisic acid-regulated anthocyanin biosynthesis. Plant Cell Environ. 2021;44:3227–45. https://doi.org/10.1111/pce.14158.
Shu P, Zhang Z, Wu Y, Chen Y, Li K, Deng H, et al. A comprehensive metabolic map reveals major quality regulations in red-flesh kiwifruit (*Actinidia chinensis*). New Phytol. 2023;238:2064–79. https://doi.org/10.1111/nph.18840.
Tan C, Wang Z, Feng X, Pan B, Irfan M, Liu C. Transcriptomic and metabolomics of flavonoid compounds in *Actinidia arguta* var. *arguta*. J King Saud Univ Sci. 2021;33:101605. https://doi.org/10.1016/j.jksus.2021.101605.
Tang D, Gallusci P, Lang Z. Fruit development and epigenetic modifications. New Phytol. 2020;228:839–44. https://doi.org/10.1111/nph.16724.
Trapnell C, Roberts A, Goff L, Pertea G, Kim D, Kelley DR, et al. Differential gene and transcript expression analysis of RNA-seq experiments with TopHat and Cufflinks. Nat Protoc. 2012;7:562–78. https://doi.org/10.1038/nprot.2012.016.
Umer MJ, Bin Safdar L, Gebremeskel H, Zhao S, Yuan P, Zhu H, et al. Identification of key gene networks controlling organic acid and sugar metabolism during watermelon fruit development by integrating metabolic phenotypes and gene expression profi les. Hortic Res. 2020;7:193. https://doi.org/10.1038/s41438-020-00416-8.
Wang R, Shu P, Zhang C, Zhang J, Chen Y, Zhang Y, et al. Integrative analyses of metabolome and genome-wide transcriptome reveal the regulatory network governing flavor formation in kiwifruit (*Actinidia chinensis*). New Phytol. 2022;233:373–89. https://doi.org/10.1111/nph.17618.
Wang S, Qiu Y, Zhu F. Kiwifruit (*Actinidia spp.*): a review of chemical diversity and biological activities. Food Chem. 2021a;350:128469. https://doi.org/10.1016/j.foodchem.2020.128469.
Wang Y, Li P, Zhu Y, Zhang F, Zhang S, He Y, et al. Graph-based pangenome of *Actinidia chinensis* reveals structural variations mediating fruit degreening. Adv Sci. 2024;11:e2400322. https://doi.org/10.1002/advs.202400322.
Wang F, Ge S, Xu X, Xing Y, Du X, Zhang X, et al. Multiomics analysis reveals new insights into the apple fruit quality decline under high nitrogen conditions. J Agric Food Chem. 2021b;69:5559–72. https://doi.org/10.1021/acs.jafc.1c01548.
Wojdyło A, Nowicka P. Anticholinergic effects of *Actinidia arguta* fruits and their polyphenol content determined by liquid chromatography-photodiode array detector-quadrupole/time of flight-mass spectrometry (LC-MS-PDA-Q/TOF). Food Chem. 2019;271:216–23. https://doi.org/10.1016/j.foodchem.2018.07.084.
Wu S, Wu D, Song J, Zhang Y, Tan Q, Yang T, et al. Metabolomic and transcriptomic analyses reveal new insights into the role of abscisic acid in modulating mango fruit ripening. Hortic Res. 2022;9:uhac102. https://doi.org/10.1093/hr/uhac102.
Wu T, Hu E, Xu S, Chen M, Guo P, Dai Z, et al. clusterProfiler 4.0: a universal enrichment tool for interpreting omics data. Innovation. 2021;2:100141. https://doi.org/10.1016/j.xinn.2021.100141.
Xie X, Li S, Zhang R, Zhao J, Chen Y, Zhao Q, et al. The bHLH transcription factor MdbHLH3 promotes anthocyanin accumulation and fruit colouration in response to low temperature in apples. Plant Cell Environ. 2012;35:1884–97. https://doi.org/10.1111/j.1365-3040.2012.02523.x.
Ye J, Li W, Ai G, Li C, Liu G, Chen W, et al. Genome-wide association analysis identifies a natural variation in basic helix-loop-helix transcription factor regulating ascorbate biosynthesis via D-mannose/L-galactose pathway in tomato. PLoS Genet. 2019;15:e1008149. https://doi.org/10.1371/journal.pgen.1008149.
Yu M, Man Y, Lei R, Lu X, Wang Y. Metabolomics study of flavonoids and anthocyanin-related gene analysis in kiwifruit (<italic>Actinidia chinensis</italic>) and kiwiberry (<italic>Actinidia arguta</italic>). Plant Mol Biol Rep. 2020;38:353–69. https://doi.org/10.1007/s11105-020-01200-7.
Zeng Z, Li Y, Zhu M, Wang X, Wang Y, Li A, et al. Kiwifruit spatiotemporal multiomics networks uncover key tissue-specific regulatory processes throughout the life cycle. Plant Physiol. 2025;197:kiae567. https://doi.org/10.1093/plphys/kiae567.
Zhang A, Zhang Q, Li J, Gong H, Fan X, Yang Y, et al. Transcriptome co-expression network analysis identifies key genes and regulators of ripening kiwifruit ester biosynthesis. BMC Plant Biol. 2020a;20:103. https://doi.org/10.1186/s12870-020-2314-9.
Zhang C, Hao YJ. Advances in genomic, transcriptomic, and metabolomic analyses of fruit quality in fruit crops. Hortic Plant J. 2020b;6:361–71. https://doi.org/10.1016/j.hpj.2020.11.001.
Zhang J, Du K, Xie Y, Zhang X, Jiang W, Li M, et al. Integration of transcriptomic and metabolomic data reveals new tetraploid kiwifruit hybrids with enhanced nutrients. LWT. 2022;170:114012. https://doi.org/10.1016/j.lwt.2022.114012.
Zhang L, Li Z, Wang Y, Jiang Z, Wang S, Huang H. Vitamin C, flower color and ploidy variation of hybrids from a ploidy-unbalanced <italic>Actinidia</italic> interspecific cross and SSR characterization. Euphytica. 2010;175:133–43. https://doi.org/10.1007/s10681-010-0194-z.
Zhang Y, Zhong C, Liu Y, Zhang Q, Sun X, Li D. Agronomic trait variations and ploidy differentiation of kiwiberries in Northwest China: implication for breeding. Front Plant Sci. 2019;8:711. https://doi.org/10.3389/fpls.2017.00711.
Zhao Y, Liu G, Yang F, Liang Y, Gao Q, Xiang C, et al. Multilayered regulation of secondary metabolism in medicinal plants. Mol Hortic. 2023;3:11. https://doi.org/10.1186/s43897-023-00059-y.
Zheng Y, Jiao C, Sun H, Rosli HG, Pombo MA, Zhang P, et al. iTAK: a program for genome-wide prediction and classification of plant transcription factors, transcriptional regulators, and protein kinases. Mol Plant. 2016;9:1667–70. https://doi.org/10.1016/j.molp.2016.09.014.
Zhu C, You C, Wu P, Huang Y, Zhang R, Fan Z, et al. The gap-free genome and multi-omics analysis of *Citrus reticulata* 'Chachi' reveal the dynamics of fruit fl avonoid biosynthesis. Hortic Res. 2024;11:uhae177. https://doi.org/10.1093/hr/uhae177.

Publisher's Note

Springer Nature remains neutral with regard to jurisdictional claims in published maps and institutional affiliations.